Experimental study of tyre/road contact forces in rolling conditions for noise prediction

Julien Cesbron, Fabienne Anfosso-Lédée, Denis Duhamel, Yin Hai-Ping, Donatien Le Houedec

Experimental study of tyre/road contact forces in rolling conditions for noise prediction

Julien Cesbron [a,*], Fabienne Anfosso-Lédée [b], Denis Duhamel [c], Hai Ping Yin [c], Donatien Le Houédec [d]

[a] *LMEE, Université d'Evry, 40 rue du Pelvoux, 91020 Evry, France*

[b] *LCPC, BP 4129, 44341 Bouguenais Cedex, France*

[c] *Université Paris-Est, UR Navier, LAMI, ENPC, 6 et 8 Avenue Blaise Pascal, Cité Descartes, Champs sur Marne, 77455 Marne la Vallée, Cedex 2, France*

[d] *ECN, GeM, 1 rue de la Noë, BP 92101, 44321 Nantes Cedex 3, France*

Abstract

This paper deals with the experimental study of dynamical tyre/road contact for noise prediction. *In situ* measurements of contact forces and close proximity noise levels were carried out for a slick tyre rolling on six different road surfaces between 30 and 50 km/h. Additional texture profiles of the tested surfaces were taken on the wheel track. Normal contact stresses were measured at a sampling frequency of 10752 Hz using a line of pressure sensitive cells placed both along and perpendicular to the rolling direction. The contact areas obtained during rolling were smaller than the one measured in statics. This is mainly explained by the dynamical properties of tyre compounds, like the viscoelastic behaviour of the rubber of the tyre tread. Additionally the root-mean-square of the resultant contact forces at various speeds was in the same order for a given road surface, while their spectra were quite different. This is certainly due to a spectral influence of bending waves propagating in the tyre during rolling, especially when the wavelength is small in comparison

Preprint submitted to Journal of Sound and Vibration *16 June 2008*

with the size of the contact patch. Finally, the levels of contact forces and close proximity noise measured at 30 km/h were correlated. Additional correlations with texture levels were performed. The results show that macro-texture linearly generates contact forces around 800 Hz and consequently noise levels between 500 Hz and 1000 Hz via the vibrations transmitted to the tyre.

Key words: Tyre/road noise, Rolling contact, Experimental methods

1 Introduction

Over the last decades the reduction of tyre/road noise has become a major issue in the struggle against road traffic noise, as related in Ref. [1]. Tyre/road noise is generated by complex mechanisms such as tyre vibrations, air-pumping and stick/slip phenomenon which are widely described in Ref. [2]. For a good prediction of these mechanisms, a reliable description of tyre/road contact interaction is of major interest.

During rolling, the road texture generates stresses in the contact patch which induce tyre vibrations and thus noise emission. Due to the difficulty to study the tyre/road contact experimentally, the investigations have been essentially focussed on the development of contact models. Many approaches have been proposed for modelling tyre/road contact stresses for noise prediction. First a Winkler bedding model coupled with the vibrations of an orthotropic plate model of the tyre belt was developed in Refs. [3–5]. The Winkler model was also used recently for a stochastic evaluation of tyre vibration in Refs. [6].

* Corresponding author : Tel: 33 6 15 19 51 65
Email address: cesbron.julien@neuf.fr (Julien Cesbron).

Alternative contact models are based on half-space assumptions for the tyre tread in the local area of tyre/road contact. The problem can be solved using a boundary element discretization [7–10], analytical multi-asperity approaches [11,12] or a mixed method taking the benefits of the analytical multi-asperity formulation for solving the boundary element problem more efficiently [13]. Finally, a finite element approach based on continuum mechanics was recently proposed in [14]. For all these models, only the normal contact forces are calculated and the friction is not taken into account. A recurrent hypothesis is also that the contact during rolling is evaluated from several contact patches in statics or quasi-statics for successive time steps. Moreover, the contact models are often validated by means of tyre vibration measurements in rolling conditions [15,16] or spindle forces and moments measurements [17], but not from dynamical contact stresses measurements.

Thus the aim of this paper is the experimental study of tyre/road contact in rolling conditions for the validation of tyre/road contact models for noise prediction. The problem is here essentially investigated from a road perspective since the contact tests were performed *in situ* for a slick tyre rolling on different road surfaces. Moreover only the normal contact stresses are measured. In a first part (Secs. 2 and 3), the contact forces measured at different speeds up to 50 km/h are used to study the dynamical effects of the tyre on the contact such as viscoelasticity and vibrations. In a second part (Sec. 4) the influence of road texture on contact forces and tyre/road noise is evaluated by means of statistical correlations between texture, contact forces and noise levels. For each part, the results are discussed by considering the complexity of the problem in connection with previous results from the literature.

2 Measurement of contact forces

2.1 Contact pressure measurement system

The normal stresses between the tyre and the road were measured at the contact interface using a real time acquisition system which is composed of a matrix-based sensor linked to a computer (Fig. 1). The sensor consists in a resistive polymer divided in sensitive cells on which the electrical resistance varies proportionally to the contact pressure. On each cell the pressure is measured in a square sensitive area smaller than the total area of the cell (see zoom in Fig. 1). Then each cell provides the mean pressure of the real pressure distribution caused by road texture within this active area. The sensor used in this study has an active area of 436×368 mm^2 and is composed of 52×44 square sensitive cells of size $h \times h$ with $h = 8.38$ mm.

Following the recommendations of the manufacturer [18], the measurement system was calibrated from the total load applied on the tyre which was measured independently on a weighting device. The variations of the response on the different cells composing the sensor are small (Ref. [18]) and can be neglected in most applications. Thus the cells were not individually calibrated (this step is called "equilibration" in [18]). The overall system accuracy is ± 10 % of the full pressure scale which varies between 0 and 0.86 MPa in this study.

The sensor is about 0.1 mm thick which minimizes the intrusion at the contact interface. However the presence of the sensor can modify the tyre/road contact properties. This issue was investigated in laboratory by measuring the contact

between a single spherical indenter and a rubber block, with or without the sensor at the interface. By comparison with the classical Hertz's theory [19], the Young's modulus of the rubber was identified from an indentation test. It was 12 % higher in presence of the sensor at the contact interface. This means that the rubber and the sensor are stiffer than the rubber alone. In the case of tyre/road contact, this will lead to stiffer contact during measurements compared with the tyre running directly on the road surface, possibly giving more uniform pressure distribution.

Concerning the sampling frequency f_s, the contact data can be acquired at 207 Hz on all the cells or at 10752 Hz on a single line of 44 cells (Fig. 1). In practice, the acquisition at 207 Hz can lead to an erroneous interpretation of data when the motion of the contact area is significantly high compared to the scanning speed of the acquisition system. Thus the 207 Hz acquisition scheme was only used for static measurements, whereas the rolling contact was studied on the single active line at 10752 Hz.

2.2 Road materials

The measurement campaign was carried out on a test track in the Laboratoire Central des Ponts et Chaussées (LCPC, Nantes, France). Six real road surfaces were used for the tests as shown in Fig. 2. Two of them are asphalt concretes with 6 mm maximum aggregate size: a Porous Asphalt (PA 0/6) and a semi-porous Thin Layer (TL 0/6). Two others are dense asphalt concretes with 10 mm maximum aggregate size: DAC 0/10 (new) and DAC 0/10 (old). The last two surfaces are a Fine Surface Dressing (FSD 0.8/1.5) and a Sand Asphalt (SA 0/4) composed of small size aggregates. It is noticed that coarse-grained

road surfaces were not included in the study due to the risk of piercing the contact sensor with such aggressive surface textures.

2.3 Experimental procedure

The contact tests were performed on a passenger car fitted with two slick tyres on the rear wheels. Contact pressures were measured on the right rear slick tyre at a constant rolling speed, as illustrated in Fig. 3. This speed was accurately measured for each test by a tachometer fixed to the wheel. It was limited to 50 km/h in order to avoid any damage to the pressure sensor but also for a correct analysis of the signals at low frequency.

As mentioned in the introduction, a first aim of the study is to investigate the differences between the tyre/road contact in statics and in rolling conditions. Thus for each road surface a contact patch was first measured in statics at 207 Hz on all cells. The sensor was taped on the road surface and calibrated as explained in Sec. 2.1. Then at the same position dynamical tests were performed by rolling at 30, 40 and 50 km/h on the active line of cells (at 10752 Hz). First measurements, denoted as "transverse tests", were performed with the active line perpendicular to the rolling direction. These tests enabled to estimate dynamical contact patches in rolling conditions (Sec. 3.2). Then measurements were performed with the active line of the sensor along the rolling direction, which are denoted as "longitudinal tests". These tests were used to investigate the variations of the dynamical contact forces with speed on the different road surfaces (Sec. 3.3).

3 Analysis of measured dynamical contact forces

3.1 Contact description

For a proper analysis of the measured data, the tyre/road contact is described in cartesian coordinates (Fig. 4). The vehicle is rolling at a constant cruising speed V in the straight line direction $(O', \mathbf{X})$ in the fixed reference frame $\mathcal{R}'=(O', \mathbf{X}, \mathbf{Y}, \mathbf{Z})$ attached to the road surface $\mathcal{S}_1$. The contact problem is projected and studied in the $(O', \mathbf{X}, \mathbf{Y})$ plane at each instant t.

The contact area $\Sigma_c(t)$ between the road surface $\mathcal{S}_1$ and the tyre tread $\mathcal{S}_2$ varies with time due to the variations of road texture and the dynamic excitation of the tyre during rolling. At time t, three sets of points can be distinguished within the contact area. The first two are the points of the road surface $\mathcal{S}_1$ and those of the tyre surface $\mathcal{S}_2$ which are coincident with $\Sigma_c(t)$. The third one is composed of the geometrical points of contact, attached to a geometrical space noted Σ, which do not belong neither to $\mathcal{S}_1$ nor to $\mathcal{S}_2$ and which is moving on both $\mathcal{S}_1$ and $\mathcal{S}_2$ during rolling. Thus for a point M in the contact area at time t, three speeds can be defined in the reference frame $\mathcal{R}'$ with respect to the considered set of points: $\mathbf{V}_{\mathcal{R}'}(M \in \mathcal{S}_1)$, $\mathbf{V}_{\mathcal{R}'}(M \in \mathcal{S}_2)$ and $\mathbf{V}_{\mathcal{R}'}(M \in \Sigma)$. Assuming rolling without sliding, the following relation occurs:

$$\forall t, \forall M \in \Sigma_c(t), \mathbf{V}_{\mathcal{R}'}(M \in \mathcal{S}_1) = \mathbf{V}_{\mathcal{R}'}(M \in \mathcal{S}_2) = \mathbf{0} \tag{1}$$

since the set of points attached to the road surface $\mathcal{S}_1$ are fixed in $\mathcal{R}'$. On the other hand, the points belonging to Σ have a uniform straight motion towards the rolling direction:

$$\forall t, \forall M \in \Sigma_c(t), \mathbf{V}_{\mathcal{R}'}(M \in \Sigma) = V\mathbf{X} \tag{2}$$

7

A second reference frame $\mathcal{R} = (O, \mathbf{x}, \mathbf{y}, \mathbf{z})$ attached to Σ is defined (Fig. 4). The point O corresponds to the orthogonal projection of the wheel center G in the $(O', \mathbf{X}, \mathbf{Y})$ plane. Then Σ is materialized by a rectangular area centered around O which dimensions $L_x \times L_y$ are fixed and include the whole contact area $\Sigma_c(t)$ at each time step. The trajectory $(X(t), Y(t))$ in $\mathcal{R}'$ of a point M of coordinates (x, y) in Σ is given by:

$$X(M \in \Sigma, t) = Vt + X_0 + x \quad \text{and} \quad Y(M \in \Sigma, t) = y + Y_0 \tag{3}$$

where (X_0, Y_0) are the coordinates of point O in $\mathcal{R}'$ at the initial time step $t_0 = 0$.

3.2 Results from the "transverse tests"

In the case of measurements in the transverse direction, the active line of the sensor is placed on the $(O', \mathbf{Y})$ axis (Fig. 5). The resultant contact force F is then obtained by integrating the measured contact pressures $p_i(t)$ at time t:

$$F(t) = h^2 \sum_{i=1}^{n_c} p_i(t) \tag{4}$$

where n_c=44 is the number of active cells. Noting $L_{yc}(t)$ the contact length in the transverse direction, then $F(t)$ represents the progressive loading of the tyre on the road within the elementary surface of length $L_{yc}(t)$ and width h. A measurement example is given in Fig. 6 for the DAC 0/10 (new) at 30 km/h. Fig. 6 (a) gives the variation of the contact pressure on each cell with time while Fig. 6 (b) gives the resultant force. This example clearly shows the progressive loading and unloading of the tyre on the active line of cells during the "transverse tests". The resultant force reaches a maximum when the center of the wheel is above the measurement line.

From the measurements, the total contact area noted A can be estimated by:

$$A = V \int_{t_1}^{t_2} L_{yc}(t)dt \tag{5}$$

where t_1 is the instant when the tyre begins to load on the line of cells and t_2 is the time when the tyre leaves it. The contact patches measured in statics and at 30, 40 and 50 km/h are given in Fig. 7 for the DAC 0/10 (new). It is noted that the dynamic contact prints are only estimated from the data measured on the active line and that the variation of texture in the rolling direction is not taken into account. The position of point O is estimated from the coordinates of the force center. The space step in the $(O, \mathbf{x})$ direction is given by $\Delta x = V\Delta t$ where Δt is the time step. The results in Fig. 7 show that the contact areas in rolling conditions are about 20 % smaller than the one in statics. Moreover the dynamic contact areas are in the same order for the three rolling speeds. The decrease of the contact area is mainly observed in the longitudinal direction, while the length in the transverse direction remains almost constant between static and dynamic data. Similar results were observed for the other five road surfaces as it can be found in Table 1.

The direct comparison of static and dynamic contact areas may be questioned since two different measurement methods have been used (matrix of cells in statics and line of cells in dynamics). A first source of error is a slight overestimation of the contact area in statics due to the size of the cells. In fact some cells in the periphery of the contact patch can be only partially loaded but will be counted as a full cell in the contact area. Another source of error in the active line technique can be due to the inhomogeneous contact properties when the tyre is partly loaded on the sensor and on the road. This transition effect might be even more important if the road is not perfectly flat in the

9

rolling direction. However this effect is expected to be small because the sensor is very thin and the evenness of the test track is of high quality. Moreover the contact length in the rolling direction measured in section 3.3 is in agreement with the results of this section.

3.3 Results from the "longitudinal tests"

In the case of the tests in the rolling direction, the active line of cells is placed on the $(O', \mathbf{X})$ axis (Fig. 8). The resultant contact force F is calculated by integrating the measured contact pressures as in Eq. (4). For the "longitudinal tests", this force is representative of the total load applied at each time step within the elementary area of length $L_{xc}(t)$ and width h, where $L_{xc}(t)$ is the contact length in the longitudinal direction at time t. Thus the resultant force "moves" with the geometric space Σ and fluctuates with the variations of the road texture during rolling.

The contact pressures measured over time at 30 km/h are given in Fig. 9 for the DAC 0/10 (old). Looking at the signal obtained for a fixed value of X gives the contact pressure measured over time on a single cell. It is representative of the loading of the tyre on a small surface of the road covered by the cell. The signal has the same shape as the resultant force observed in Fig. 6 for the "transverse tests". The cells with no signal are cells without contact, but errors in the cells can also appear like the third last cell which shows a contact pressure and then a loss of contact. Now, looking at the contact pressures measured simultaneously on different cells in Fig. 9, it is observed that the contact patch go forward with time following the motion of the tyre on the measurement line at speed V. The number of loaded cells at each time step

10

enables to evaluate the contact length $L_{xc}(t)$. On average for the six tested road surfaces, the contact length was 88 ± 4 mm at 30 km/h, 85 ± 3 mm at 40 km/h and 88 ± 5 mm at 50 km/h. These values are close to 90 mm and the fact that the contact length is almost invariant with the speed are in agreement with the results on the contact areas observed in Sec. 3.2.

Integrating the contact pressures of Fig. 9 at each time step gives the resultant force F in the case of the "longitudinal tests". The resultant forces obtained for the DAC 0/10 (old) at 30, 40 and 50 km/h are represented in Fig. 10 (a). The same signals are plotted in Fig. 10 (b) using Vt instead of t as a variable. In this case, it appears that the signals are very similar for the three rolling speeds, which may be explained by the fact that the measured contact forces are mainly influenced by the position $X_0 + Vt$ of the tyre on the road, i.e. by the texture of the road surface. The same observations were made for the other five road surfaces. Then in the following the root-mean-square resultant forces and the spectral content of the signals at different speeds are compared in order to confirm that the variations of the contact force are mainly due to the position on the road or if dynamics of the tyre has an effect.

If the resultant force is mainly influenced by the road texture, then at different speeds V_i the resultant forces F_i can be written as an invariant function g of the variable $V_i t$ representative of the position $X(O,t) = X_0 + V_i t$ of the tyre on the road surface. This approximation gives:

$$\forall t \in [0, T_i], \quad F_i(t) = g(V_i t) \tag{6}$$

where $t_0 = 0$ is the instant when the tyre enters onto the active line of cells and T_i is the time when the tyre leaves it at speed V_i. Then under the assumption of

11

Eq. (6) the root-mean-square (rms) resultant force $F_{rms,i}$ at speed V_i satisfies:

$$F_{rms,i} = \sqrt{\frac{1}{T_i}\int_0^{T_i} |F_i(t)|^2 dt} = \sqrt{\frac{1}{V_i T_i}\int_0^{V_i T_i} |g(X)|^2 dX} \tag{7}$$

Additionally the length $L = V_i T_i$ remains invariant with the speed due to the fact that the tyre always crosses the same finite length of the active line of cells:

$$\forall V_i, \quad V_i T_i = L \tag{8}$$

Introducing the relation of Eq. (8) into Eq. (7) finally leads to:

$$F_{rms,i} = \sqrt{\frac{1}{L}\int_0^{L} |g(X)|^2 dX} = g_{rms} \tag{9}$$

where g_{rms} is the rms value of function g and should be invariant with speed due to the fact that the tyre always crosses the same profile of the road texture for the three tests at different speeds. Thus for a given road surface the rms resultant forces $F_{rms,i}$ should be the same at different speeds. Also for the six tested road surfaces, the rms resultant forces $F_{rms,i}$ were calculated from the measured signals. The values of $F_{rms,30}$ and $F_{rms,40}$ obtained respectively at 30 and 40 km/h and those of $F_{rms,30}$ and $F_{rms,50}$ obtained respectively at 30 and 50 km/h are compared in Fig. 11. On each graph, the data from the six road surfaces were considered and a linear fitting was performed. This gives a regression line (in plain line) which coefficients a and b are given in the top left. A good agreement between the rms forces was found in both cases as attested by the value of the correlation coefficient ρ very close to one.

Another consequence of Eq. (6) is that the Fourier transform $\hat{F}_i$ of the resultant force measured at speed V_i should be linked to the Fourier transform $\hat{g}$ of the function g by:

$$\hat{F}_i(f) = \int_0^{T_i} F(t) e^{-2\pi i f t} dt = \frac{1}{V_i}\int_0^{L} g(X) e^{\frac{-2\pi i f X}{V_i}} dX = \frac{\hat{g}(f/V_i)}{V_i} \tag{10}$$

12

where f is the frequency. Then from Eq. (10) the Fourier transform of a force F_r measured at a reference speed V_r and the one of a force F_i measured at a speed V_i are linked by:

$$V_r \hat{F}_r(f) = V_i \hat{F}_i(f V_i / V_r) \tag{11}$$

Additionally the spectral levels $L_{F,i}$ of the contact force measured at the speed V_i are calculated as follows:

$$L_{F,i}(f) = 20 \log_{10} \left(\frac{|\hat{F}_i(f)|}{F_0} \right) \tag{12}$$

where $|\hat{F}_i(f)|$ is the modulus of $\hat{F}_i(f)$ and $F_0 = 10^{-3}$ N is a reference force value which allows to get force levels between 0 and 120 dB. Then the modified spectral levels $L^*_{F,i}$ at speed V_i are defined by:

$$L^*_{F,i}(f) = L_{F,i}(f) + 20 \log_{10}(V_i) \tag{13}$$

Finally, from Eqs. (11) and (13) the following relation should be verified under the assumption of Eq. (6):

$$L^*_{F,r}(f) = L^*_{F,i}(f V_i / V_r) \tag{14}$$

The spectra $L^*_{F,i}(f V_i / V_r)$ at 30, 40 and 50 km/h are given in Fig. 12 (a) for the DAC 0/10 (old). The reference speed V_r is 30 km/h and the levels are represented between 0 and 2500 Hz. On the figure, the value of $L^*_{F,i}(f V_i / V_r)$ is plotted at frequency f, based on Eq. (14). For instance at f=100 Hz the levels $L^*_{F,30}$(100 Hz), $L^*_{F,40}$(133 Hz) and $L^*_{F,50}$(166 Hz) are plotted for the three speeds. The levels are relatively close at low frequencies but the comparison are not good at high frequencies using this representation. The same spectra are plotted in third octave bands in Fig. 12 (b). The results are quite different both in terms of shape and amplitude. Some similarities can be observed below

13

315 Hz, especially for the signal at 40 km/h and 50 km/h. However the levels at the different speeds are significantly different at frequencies above 315 Hz. Similar results were obtained for the other road surfaces.

3.4 Discussion

The results obtained from the measurements of the dynamical contact stresses can be summarized as follows:

(1) The contact area in rolling conditions remains almost constant with speed and is 20 % smaller than the one measured in statics. The decrease is mainly observed for the contact length in the rolling direction.
(2) The rms resultant force for the "longitudinal tests" is almost invariant with speed.
(3) The force spectra for the "longitudinal tests" vary widely with speed.

The three points mentioned above are linked to the rolling speed and are observed for all tested road surface. Therefore in the following the results are discussed from the dynamic of the tyre rather than the properties of the road surface. The geometry of the road surface (shape, size and distribution of the asperities) has a great influence on tyre/road contact too, but this will be discussed in section 4.

The decrease of the contact area (1) can be due to the centrifugation of the tyre belt during rolling and to the dynamical material properties of tyre compounds. Rotation generates centrifugal and Coriolis acceleration which influences the dynamical response of the tyre. This has been widely studied in the literature from analytical or numerical tyre models. Early works [20–22] using

14

ring models have shown that the Coriolis acceleration induces a bifurcation effect on the natural frequencies of the tyre. Using cylindrical shell models, more recent works [23–25] have shown that the main influence of rotation is a Doppler shift of the dispersion curve. Models based on finite element formulation [14,26,27] also include the dynamic of the rotating tyre. A conclusion from [23] is that the stiffening of the tread due to the centrifugal force is small. This stiffening effect was experimentally studied in [17] and was associated with the increase of the vertical resonance frequency of the tyre when the rolling speed increases (2.4 Hz per 10 km/h). However, in the present study, no significant decrease of the contact area was observed with increasing speed, which means that the stiffening of the tread due to centrifugation doesn't have a significant effect on the contact areas within the studied range of speeds. The differences in the contact areas are mainly observed between static loading and rolling conditions. Thus the decrease of the contact area in rolling conditions could rather be explained by the complex dynamical properties of tyre compounds. The tyre tread is made of carbon black/silica filled rubber which has a viscoelastic behaviour. The stress/strain relation of such filled rubber is highly frequency and temperature dependent which can be described via the WLF law [28]. It is also amplitude dependent as related by Payne [29] (or Flechter and Gent [30]) in small deformations or by Mullins [31] under large deformations. The viscoelasticity has been introduced in tyre models developed for noise prediction. A Kelvin-Voigt viscoelasticity is used for describing the behaviour of the tyre in [32]. Many tyre models, like ring models [33,34], orthotropic plate models [3,35,36] or double layer plate model [37,38], use a complex modulus with the Young's modulus as a real part and loss modulus as imaginary part for taking into account the energy dissipated by rubber compounds. Frequency dependent dynamic stiffness and damping can be in-

15

troduced in the models like in [38,39] for better agreement with experimental data. A possible explanation of result (1) is that the viscoelastic behaviour tends to make the material stiffer when rolling which leads to smaller contact areas in dynamics. In other words the rubber compounds of the tyre can creep longer in statics than in dynamics, giving larger contact areas in the first case.

Results (2) and (3) relate to a strong tyre/road interaction and coupling at the contact interface. Result (2) is "texture driven" while result (3) is "tyre dynamics driven". This can be discussed from results of the literature concerning tyre vibrations and numerical tyre/road contact models. The differences in the force spectra at different speeds could be due to the vibration of the tyre tread during rolling. From tyre models mentioned above three wave types can propagate in the tyre structure during rolling (Ref. [37]), which are bending waves, longitudinal waves and in-plane (or rotational) waves. The dispersion relations for these waves are influenced by the material properties, the external tension in the tyre belt and the inflated pressure. Since longitudinal and in-plane waves do not have a significant amplitude in the radial direction, only the vibrations due to bending waves have a strong influence on the normal contact stresses. Here idealized bending waves are considered to make the interpretation easier. For instance, considering the results of Ref. [37], the velocity of the bending waves travelling the tyre, noted c, is about 80 m.s^{-1} between 500 and 1000 Hz. Thus at 500 Hz the wavelength $\lambda = c/f$ is about 160 mm which is close to the length of the contact patch in the transverse direction. Also the observed differences could demonstrate that when the wavelength associated with the vibrations in the tyre is small in comparison with the dimensions of the contact patch (i.e. $\lambda < 160$ mm) then the contact in rolling conditions is highly different from the contact in statics. On the contrary the dynamical contact

16

may be approached by quasi-static states at low frequencies. The influence of tyre vibrations on the contact stresses was also exemplified by the results of tyre/road contact models. Contact models based on Winkler bedding or elastic half-space coupled with the vibration of a tyre model (orthotropic plate [3,15] or double layer plate [9]) give good correlations with experimental spectral data regarding resulting vibrations (Ref. [15]). Thus the vibration of the tyre is an important parameter in the calculation of the resultant contact force.

4 Correlation of contact forces with tyre/road noise

4.1 Experimental procedure including close proximity noise measurements

The aim of the measurements was here to study the relation between the contact forces from the "longitudinal tests", the road texture and the tyre/road noise by means of statistical correlations between third octave levels.

For significant comparisons with texture and noise, only the part of the force signal corresponding to the time when the tyre is entirely loaded on the active line of cells was considered. The partial loading parts of the signal (at the beginning and at the end in Fig. 10) were removed and consequently the duration of the signal was shorter. Therefore the study was carried out at 30 km/h which enables a frequency analysis in third octave bands from 400 Hz to 5000 Hz. The first limit is related to the duration of the signal (a criteria of at least three narrow band levels per third octave band was chosen) and the last limit is given by applying the Nyquist-Shannon sampling theorem. Due to the length of the active line of cells, the records are relative to texture profile samples of about 40 cm. This includes at least 40 road asperities which

17

is assumed to be enough for a statistical description of the road surface.

Texture measurements were taken by means of a laser profilometer. The sensor measuring range is ± 30 mm with a vertical resolution of ± 0.05 mm. On each test surface, 12 texture profiles of 1.2 m length were sampled every 0.1 mm along the wheel track. The space between the individual profiles was 1 m. Each texture profile was signal processed following ISO Technical Specification 13473-4 [40] to get the texture power spectrum L_T (in dB ref. 10^{-6} m) in third-octave wavelength bands. Texture spectral components were expressed in 21 third-octave bands, ranging from center wavelength λ_T of 2.5 mm up to 250 mm. These limits are related to the length of the profile and to the spatial sampling of the measurements. The final texture spectrum representative of the road surface is obtained by averaging the spectra of the 12 profiles.

Tyre/road noise was measured with a Close Proximity (CPX) method (Fig. 13). Two microphones are mounted close to the tyre/road contact zone of a test vehicle, at positions defined in ISO CD 11819-2 [41], i.e. 20 cm from the sidewall of the tyre, 20 cm from the wheel axis and 10 cm above the road surface. The test tyre is the same slick tyre as for the contact pressure measurements. The microphones are fitted with standard windshield. It has been shown that the tyre/road noise levels measured in such open field conditions are dominant on aerodynamic noise for vehicle speeds up to 110 km/h [42]. Sound pressure levels and vehicle speed are evaluated every wheel rotation, i.e. approximately every 2 meters, and averaged on 30 meter long sections centered around the spot of contact measurements on the road surface. For a better accuracy, the noise measurements are repeated three times and averaged on the lateral microphones. At each run, the sections are accurately located thanks to an infra-red sensor located on the car body that starts the

18

acquisition automatically when a retro-reflecting post is met on the road side.

For the six road surfaces three contact force measurements were performed at 30 km/h according to the "longitudinal tests" procedure. After having removed the pressure sensor, three close proximity noise measurements were then carried out at 30 km/h with the engine turned off. A preliminary study has shown that the tyre/road noise remains dominant under these conditions. It was checked that the speed of the vehicle was reasonably constant on 30 meter long sections despite the absence of power. Finally, it is noticed that the contact measurements and the acoustic tests were not performed simultaneously, but in similar meteorological conditions. The texture profiles were measured independently and not exactly at the points of contact force measurement.

4.2 Results

Statistical correlations between contact force, road texture and tyre/road noise levels were calculated from the measurements described in Sec. 4.1. The texture spectra for the six tested road surfaces are given in Fig. 14. The measured levels L_T clearly show that the PA and TL road surfaces have the higher macro-texture, while DAC road surfaces have moderate macro-texture and FSD and SA have small macro-texture. Then the third octave force levels L_F obtained by averaging the spectra of three resultant contact forces are given in Fig. 15 for the six road surfaces. Note the difference of $20\log_{10}(V)$ between the levels of Figs. 12 and 15 for the DAC 0/10 (old) at 30 km/h due to the fact that Fig. 12 gives the modified spectrum (Eq. (13)) whereas Fig. 15 gives the normal spectrum (Eq. (12)). The large differences obtained in the spectra show that at a given speed (here 30 km/h) the road surface has a great influence

on the spectral contents of the contact forces. Finally, the third octave noise levels L_N obtained at 30 km/h for the six road surfaces are given in Fig. 16. Qualitatively the surfaces with high macro-texture (PA, TL and DAC (old)) are the noisiest between 500 Hz and 1000 Hz while the fine surface dressing (FSD) is the quietest. It is noted that the standard deviation of the data for a single road surface over the full spectral range is about ± 2.1 dB for texture data, ± 1.9 dB for the contact force data and ± 0.3 dB for the noise data.

In the following the frequency corresponding to the force is noted f_F and the frequency associated with the noise is noted f_N. For each couple of frequencies (f_F, f_N), the correlation coefficient ρ between the contact force levels and the noise levels was calculated using the spectral data of Figs. 15 and 16. This is illustrated on Fig. 17 (a) for f_F= 800 Hz and f_N=800 Hz and for which the correlation coefficient is equal to 0.99. The correlation curves obtained in the (f_F, f_N) plane at 30 km/h are represented in Fig. 17 (b). It is clearly observed that the noise levels between 500 and 1000 Hz are positively correlated with the contact force levels at 800 Hz. Additional correlations were performed between the texture levels and the contact forces levels (Fig. 18) and between the texture levels and the noise levels (Fig. 19). The contact force levels at 800 Hz are positively correlated with the texture levels between 4 and 100 mm and no negative correlation is observed at high frequency. The noise levels are positively correlated between 500 and 1000 Hz with the texture levels between 4 and 160 mm and negatively correlated above 1600 Hz with small wavelengths. These texture/noise correlations are in agreement with previous results of the literature [8,43–45] for patterned tyres.

4.3 Discussion

The experimental results of Sec. 4.3 at 30 km/h can be summarized as follows:

(1) The noise levels between 500 and 1000 Hz are positively correlated with the contact force levels at 800 Hz (Fig. 17).
(2) Macro-texture has a great influence on the spectral content of the contact forces, especially around 800 Hz (Fig. 18).

A frequency of 800 Hz at 30 km/h corresponds to a texture wavelength $\lambda_T = V/f_F$ of 10 mm, which is in the order of the highest size of the aggregates composing the tested road surfaces. However the positive correlation of the force at 800 Hz was found on a wide wavelength range between 4 and 100 mm, which contains but is not exactly 10 mm. The road surfaces with high macro-texture will linearly generate higher contact forces around 800 Hz and consequently higher noise levels between 500 Hz and 1000 Hz via the vibrations transmitted to the tyre. The poor correlation of normal contact forces with noise at high frequency is in agreement with the fact that high frequency noise is generated by air-pumping or tangential contact forces (friction) which were not measured in this study.

5 Conclusions

This study is a first approach to investigate experimentally the tyre/road contact stresses in rolling conditions within the framework of tyre/road noise. *In situ* measurements of contact stresses and close proximity noise levels have been performed with a slick tyre rolling on six different road surfaces between

21

30 and 50 km/h. Additional texture profiles of the tested surfaces were measured on the wheel track. The resulting database has been used to investigate both the effects of the tyre behaviour on the dynamical contact forces and to correlate spectral contact force levels with texture and noise levels.

The dynamical contact patches obtained from the "transverse tests" show a decrease in the order of 20 percents of the contact area in rolling conditions in comparison with the one measured in statics. The poor influence of speed on the dynamical contact areas leads to the conclusion that the decrease is due to the viscoelasticity of the tyre rather than a centrifugation effect. This could be investigated further by using tyres with different viscoelastic properties or from numerical contact models where the viscoelasticity is taken into account. Concerning the "longitudinal tests", the rms value of the resultant force was almost invariant with speed for the whole tested road surfaces. On the contrary the force spectra were widely different. This is certainly due to an influence of tyre vibrations at the contact interface (bending waves) when the wavelength becomes smaller than the length of the contact patch. These results are in agreement with those from tyre/road contact models in the literature and may be completed by additional numerical or experimental studies, enabling longer length of contact signals for better spectral accuracy.

The statistical correlations in Sec. 4 show that at 30 km/h the levels of the resultant contact forces around 800 Hz are positively correlated with the texture wavelengths between 4 and 100 mm and with the noise levels between 500 and 1000 Hz. Additionally the spectral correlations between road texture and tyre/road noise are in agreement with those of the previous literature for a slick tyre. Moreover at 30 km/h the frequency of 800 Hz corresponds to a texture wavelength around 10 mm which is the maximal size of the ag-

22

gregates composing the tested road surfaces. A main conclusion is that the surface macro-texture has a linear influence on the contact forces around 800 Hz and consequently on the medium frequency noise levels via the vibrations transmitted to the tyre.

These experimental conclusions could be used to improve the existing tyre/road contact models. First a realistic description of the road surface is needed, which is already the case in most of the deterministic or hybrid models given in references. Then the tyre behaviour has to be included in the contact models. This is already the case for instance in Refs. [3,4,9,15] where the vibrations of a tyre model including frequency dependent storage and loss modulus of material compounds are coupled with the contact conditions for the calculation of contact forces. The introduction of viscoelasticity and tyre vibrations is in progress in the contact model developed by the authors (Refs. [12,13]). The improved model could be used in future works for the prediction of contact stresses in rolling conditions. The calculations could be compared with the experimental results of this study and correlated with the noise levels measured at rolling speeds above 30 km/h.

Acknowledgments

The authors thank Y. Pichaud and J.-F. Le Fur of the Laboratoire Central des Ponts et Chaussées for their technical help during the experiments. Texture measurements were carried out in the frame of the Deufrako P2RN project.

23

References

[1] U. Sandberg, Tyre/road noise - Myths and realities, *Proceedings of Internoise 2001*, The Hague, The Netherlands, August 2001, CD-ROM.

[2] U. Sandberg, J.A. Ejsmont, *Tyre/road noise reference book*, Informex, Kisa, Sweden, 2002.

[3] W. Kropp, Ein Modell zur Beschreibung des Rollgeräusches eines unprofilierten Gürtelreifens auf rauher Strassenoberfläche, PhD Thesis, T.U. Berlin, 1992.

[4] J.-F. Hamet, P. Klein, Road texture and tire noise, *Proceedings of Internoise 2000*, Nice, France, August 2000, CD-ROM.

[5] J-F. Hamet, P. Klein, Use of a rolling model for the study of the correlation between road texture and tire noise. *Proceedings of Internoise 2001*, The Hague, The Netherlands, 2001, CD-ROM.

[6] E. Rustighi, S.J. Elliott, Stochastic road excitation and control feasibility in a 2D linear tyre model. *Journal of Sound and Vibration* 300 (2007) 490-501.

[7] T.G. Clapp, A.C. Eberhardt, C.T. Kelley, Development and validation of a method for approximating road surface texture-induced contact pressure in tire-pavement interaction. *Tire Science and Technology* 16 (1988) 2-17.

[8] P. Klein, J.-F. Hamet, F. Anfosso-Lédée, An envelopment procedure for tire/road contact, *Proceedings of the 5^{th} Symposium on Pavement Surface Characteristics SURF 2004*, PIARC, Toronto, Canada, June 2004, CD-ROM.

[9] K. Larsson, Modelling of dynamic contact - Exemplified on tyre/road interaction, PhD Thesis, Chalmers University of Technology, Göteborg, Sweden, 2002.

[10] F. Wullens, Excitation of tyre vibrations due to tyre/road interaction, PhD Thesis, Chalmers University of Technology, Göteborg, Sweden, 2004.

[11] T. Fujikawa, H. Koike, Y. Oshino, H. Tachibana, Definition of road roughness parameters for tire vibration noise control. *Applied acoustics* 66 (2005) 501-512.

[12] A. Sameur, Modèle de contact pneumatique/chaussée pour la prévision du bruit de roulement, PhD thesis, École Nationale des Ponts et Chaussées, 2004.

[13] J. Cesbron, Influence de la texture de chaussée sur le bruit de contact pneumatique/chaussée, PhD Thesis, École Centrale de Nantes/Université de Nantes, 2007.

[14] M. Brinkmeier, U. Nackenhorst, S. Petersen, O. von Estorff, A finite element approach for the simulation of tire rolling noise. *Journal of Sound and Vibration* 309 (2008) 20-39.

[15] F. Wullens, W. Kropp, A three-dimensional contact model for tyre/road interaction in rolling conditions, *Acta Acustica united with Acustica* 90 (2004) 702-711.

[16] J. Périsse, A study of radial vibrations of a rolling tyre for tyre-road noise characterisation, *Mechanical Systems and Signal Processing*, 16 (2002) 1043-1058.

[17] P. Kindt, F. De Coninck, P. Sas, W. Desmet, Test setup for tire/road noise caused by road impact excitations: first outlines, *Proceedings of ISMA 2006*, Leuven, Belgium, September 2006, pp.4327-4336.

[18] Tekscan, Inc. I-Scan® Pressure Measurement System - User Manual, Version 5.7x. South Boston, 2005.

[19] H. Hertz, Über die Berührung fester elastischer Körper, *J. Reine und Angewandte Mathematik* 92 (1882) 156-171.

[20] S.C. Huang, W. Soedel, Effects of Coriolis acceleration on the free and forced in-plane vibrations of rotating rings on elastic foundation, *Journal of Sound and Vibration* 115 (2) (1987) 253-274.

[21] S.C. Huang, C.K. Su, In-plane dynamics of tires on the road based on an experimentally verified rolling ring model, *Vehicle System Dynamics* 21 (1992) 247-267.

[22] S.C. Huang, The vibration of rolling tyres in ground contact, *International Journal of Vehicle Design* 13 (1992) 78-95.

[23] Y.-J. Kim, J.S. Bolton, Effects of rotation on the dynamics of a circular cylindrical shell with application to tire vibration, *Journal of Sound and Vibration* 275 (2004) 605-621.

[24] R.J. Pinnington, A wave model of a circular tyre. Part 1: belt modelling, *Journal of Sound and Vibration* 290 (2006) 101-132.

[25] R.J. Pinnington, A wave model of a circular tyre. Part 2: side-wall and force transmission modelling, *Journal of Sound and Vibration* 290 (2006) 133-168.

[26] U. Nachenhorst, The ALE-formulation of bodies in rolling contact: theoretical foundations and finite element approach, *Computer Methods in Applied Mechanics and Engineering* 193 (2004) 4299-4322.

[27] I. Lopez, R.E.A. Blom, N.B. Roozen, H. Nijmeijer, Modelling vibrations on deformed rolling tyres - a modal approach, *Journal of Sound and Vibration* 307 (2007) 481-494.

[28] M.L. Williams, R.F. Landel, J.D. Ferry, The temperature dependence of relaxation mechanisms in amorphous polymers and other glass-forming liquids, *Journal of the American Chemical Society* 77 (1955) 3701-3707.

[29] A.R. Payne, The dynamic properties of carbon black-loaded natural rubber vulcanizates. Part I, *Journal of Applied Polymer Science* 6 (1962) 5763.

[30] W.P. Fletcher, A.N. Gent, Non-linearity in the dynamic properties of vulcanised rubber compounds, *Trans. Inst. Rubber Ind.* 29 (1953) 266280.

[31] L. Mullins, Softening of rubber by deformation, *Rubber Chemistry and Technology* 42 (1969) 339-361.

[32] J. Padovan, On viscoelasticity and standing waves in tires, *Tire science and technology* 4 (4) (1976) 233-246.

[33] W. Kropp, Structure-borne sound on a smooth tyre, *Applied Acoustics* 20 (1989) 181-192.

[34] J. Périsse, J.-F. Hamet, A comparison of the 2D ring and 3D orthotropic plate for modelling of radial tire vibrations, *Proceedings of Internoise 2000*, Nice, France, August 2000, pp.1221-1225.

[35] J.-F. Hamet, Tire/road noise : Time domain Green's function for the orthotropic plate model. *Acta acustica - Acustica* 87 (2001) 470-474.

[36] J.M. Muggleton, B.R. Mace, M.J. Brennan, Vibrational response prediction of a pneumatic tyre using an orthotropic two-plate wave model, *Journal of Sound and Vibration* 264 (2003) 929-950.

[37] K. Larsson, W. Kropp, A high-frequency three-dimensional tyre model based on two coupled elastic layers, *Journal of Sound and Vibration* 253 (2002) 889-908.

[38] P. Andersson, K. Larsson, Validation of a high frequency three-dimensional tyre model, *Acta Acustica united with Acustica* 91 (2005) 121-131.

[39] J. Svensson, P. Andersson, Identification of complex moduli for rubber compounds by minimisation of the error between measured and FE-modelled velocity profiles, *Proceedings of Euronoise 2006*, Tampere, Finland, June 2006, CD-ROM.

[40] International Organization for Standardization ISO TS 13473-4, Characterization of pavement texture by use of surface profiles - Part 4: Spectral analysis of texture profile, Geneva, Switzerland, 2000.

[41] International Organization for Standardization ISO CD 11819-2, Acoustics: Measurement of the influence of road surfaces on road traffic noise Part 2: the close-proximity method, Geneva, Switzerland, 2000.

[42] F. Anfosso-Lédée, The development of a new tire-road noise measurement device in France, *Proceedings of the 5th Symposium on Pavement Surface Characteristics SURF 2004*, PIARC, Toronto, Canada, June 2004, CD-ROM.

[43] U. Sandberg, G. Descornet, Road surface influence on tire/road noise, *Proceedings of Internoise 1980*, Miami, Florida, December 1980, pp.1-16.

[44] F. Anfosso-Lédée, M.-T. Do, Geometric descriptors of road surface texture in relation to tire-road noise. *Journal of the Transportation Research Board - Assessing and Evaluating Pavements* 1806 (2002) 160-167.

[45] P. Klein, J-F. Hamet, The correlations between texture related quantities and the tyre radiated noise levels evaluated from a dynamic rolling model, *Proceedings of Euronoise 2006*, Tampere, Finland, June 2006, CD-ROM.

List of Figures

List of Tables

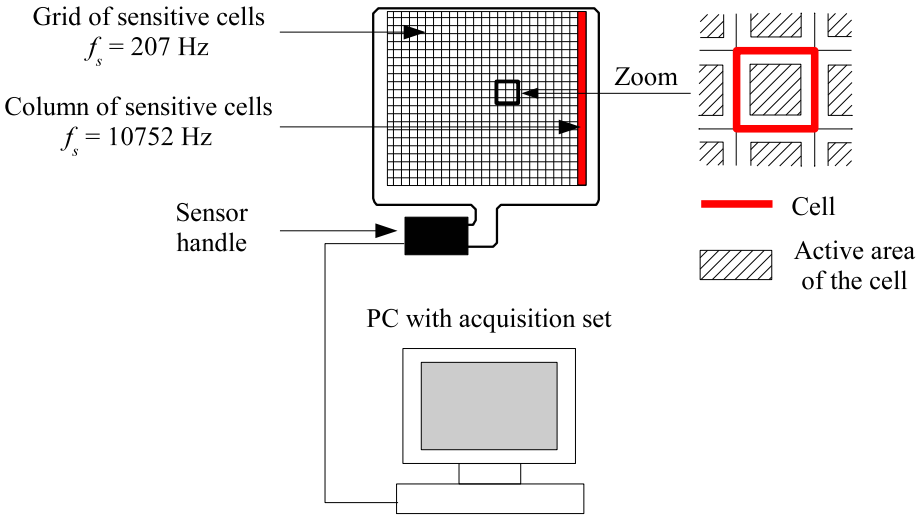

Fig. 1. Schematic view of the dynamical pressure measurement system.

31

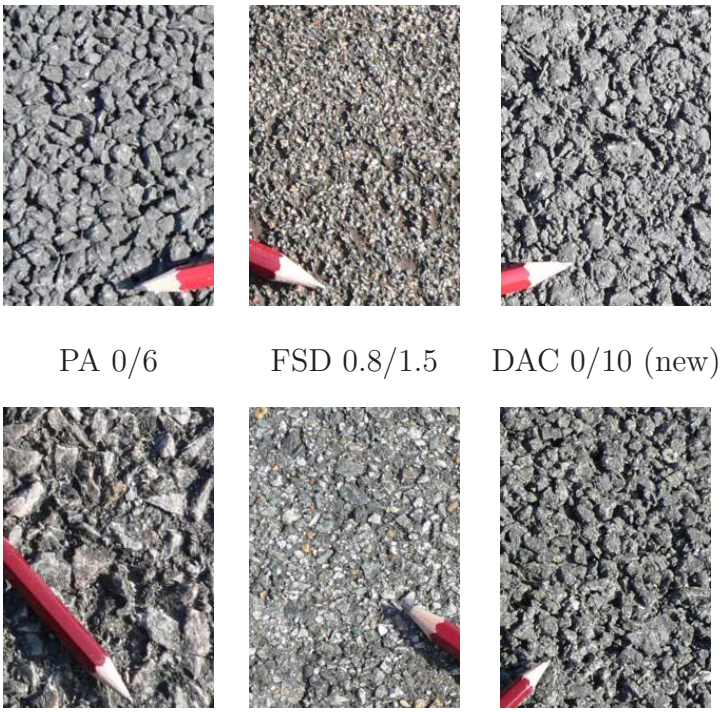

Fig. 2. Upper view of the six surfaces used for the tests.

32

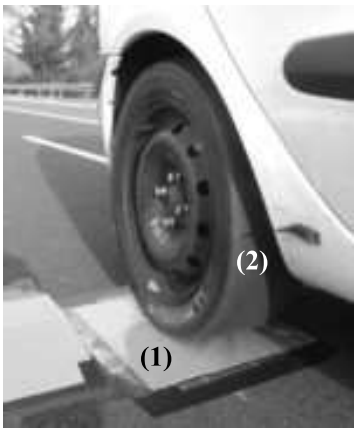

Fig. 3. *In situ* contact forces measurement ((1) pressure sensitive device, (2) slick tyre).

33

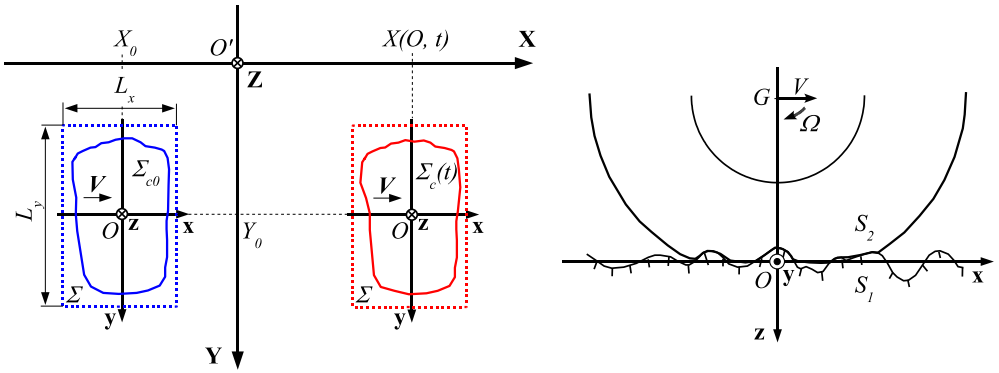

Fig. 4. Description of contact kinematics.

34

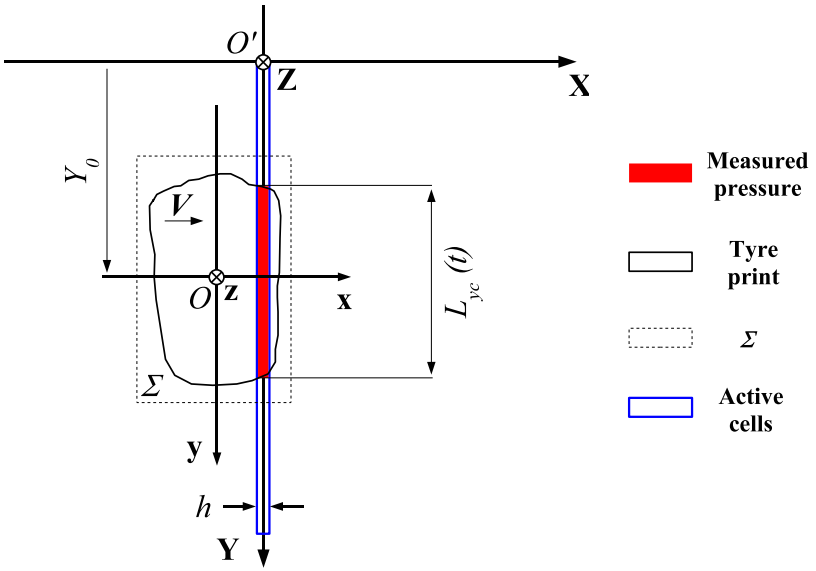

Fig. 5. Position of the active line of cells for the "transverse tests".

35

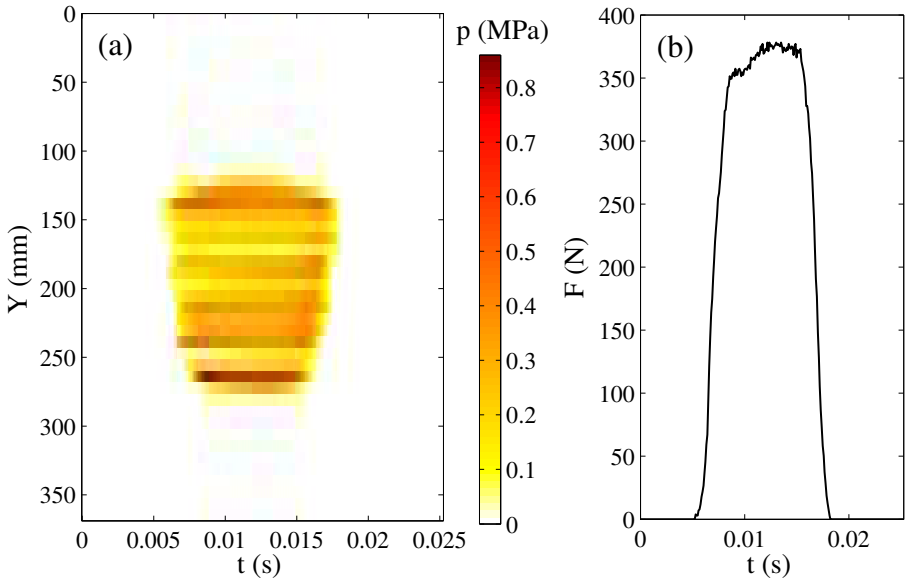

Fig. 6. Measurement at 30 km/h for the DAC 0/10 (new) road surface in the case of the "transverse tests": (a) Contact pressures, (b) Resultant contact force F.

36

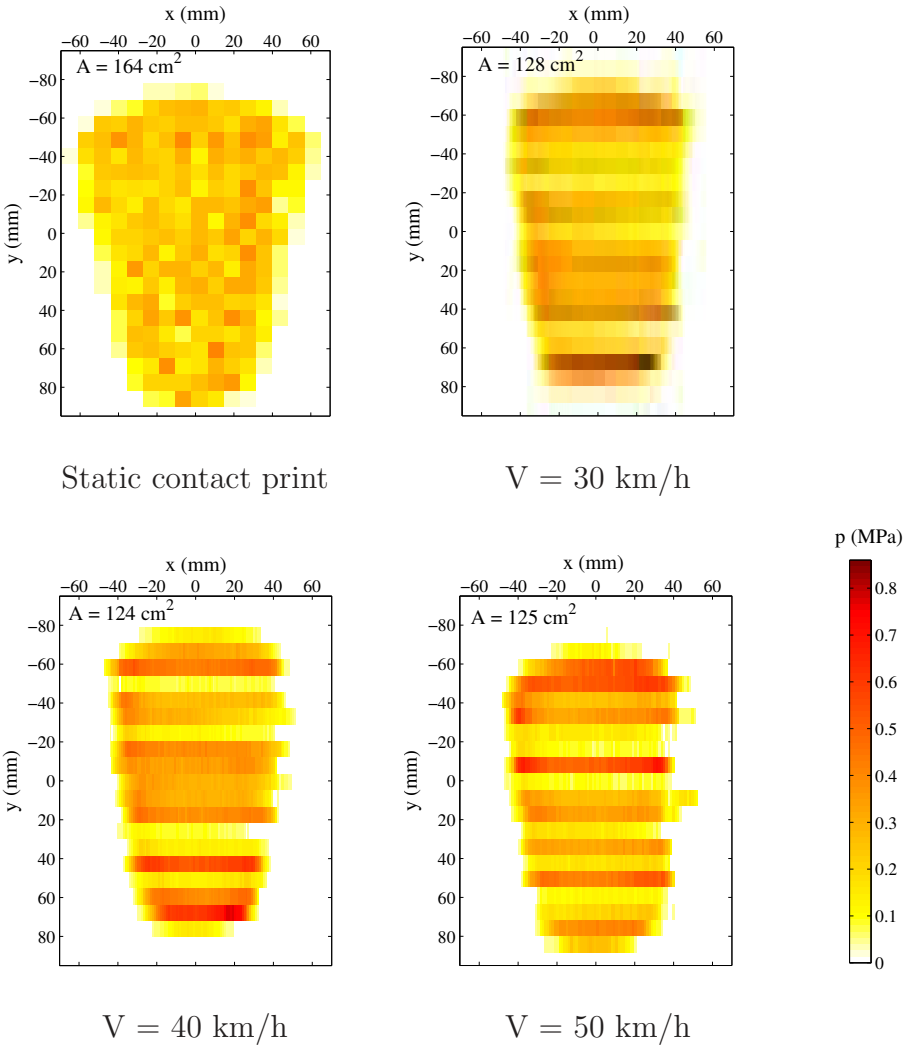

Fig. 7. Contact patches measured in statics and reconstructed from the "transverse tests" at 30, 40 and 50 km/h for the DAC 0/10 (new) road surface.

37

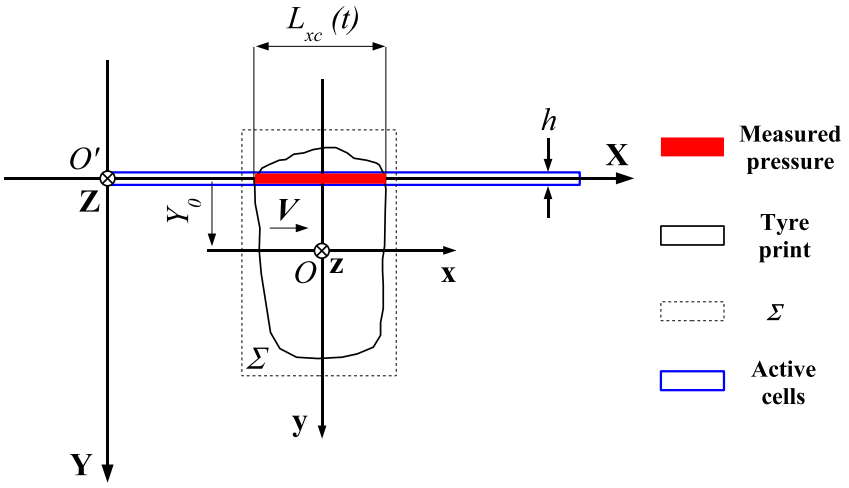

Fig. 8. Position of the active line of cells for the "longitudinal tests".

38

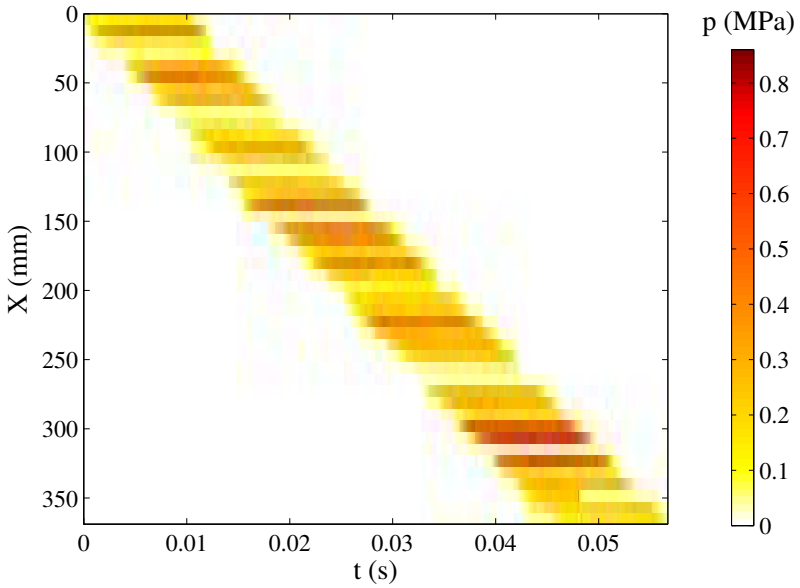

Fig. 9. Contact pressures measured at 30 km/h for the DAC 0/10 (old) road surface in the case of the "longitudinal tests".

39

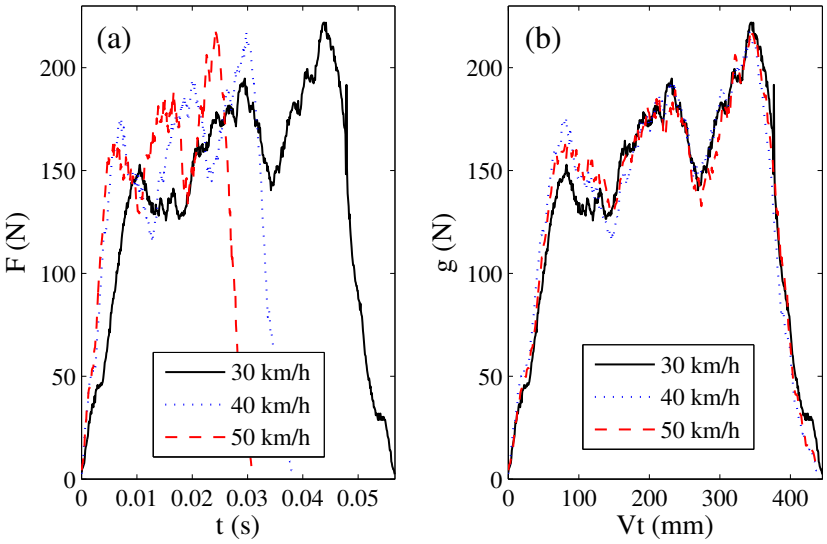

Fig. 10. Contact forces obtained from the "longitudinal tests" at 30, 40 and 50 km/h for the DAC 0/10 (old) road surface: (a) Resultant contact forces $F(t)$, (b) Associated functions $g(Vt)$.

40

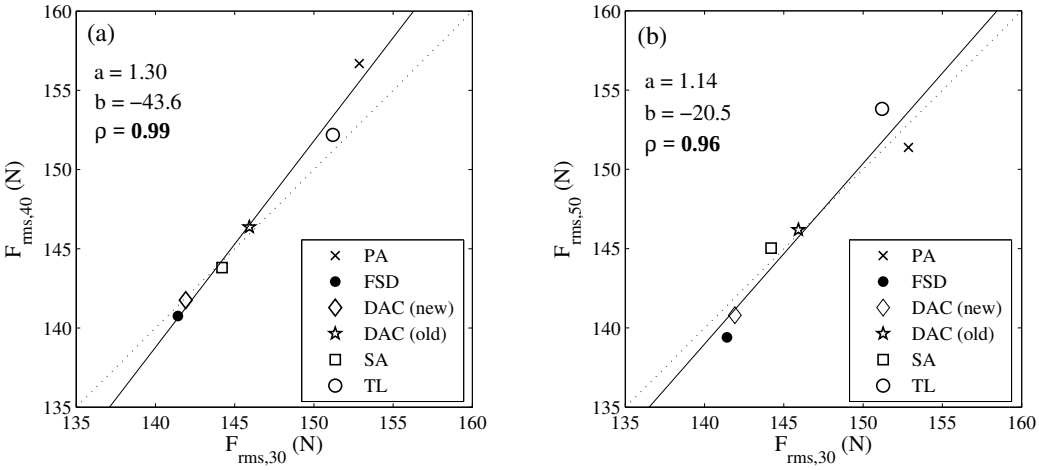

Fig. 11. Comparison of the rms resultant forces $F_{rms,i}$ obtained at different speeds from the "longitudinal tests". (a) $F_{rms,40}$ versus $F_{rms,30}$, i.e. the rms forces at 30 and 40 km/h. (b) $F_{rms,50}$ versus $F_{rms,30}$, i.e. the rms forces at 30 and 50 km/h.

41

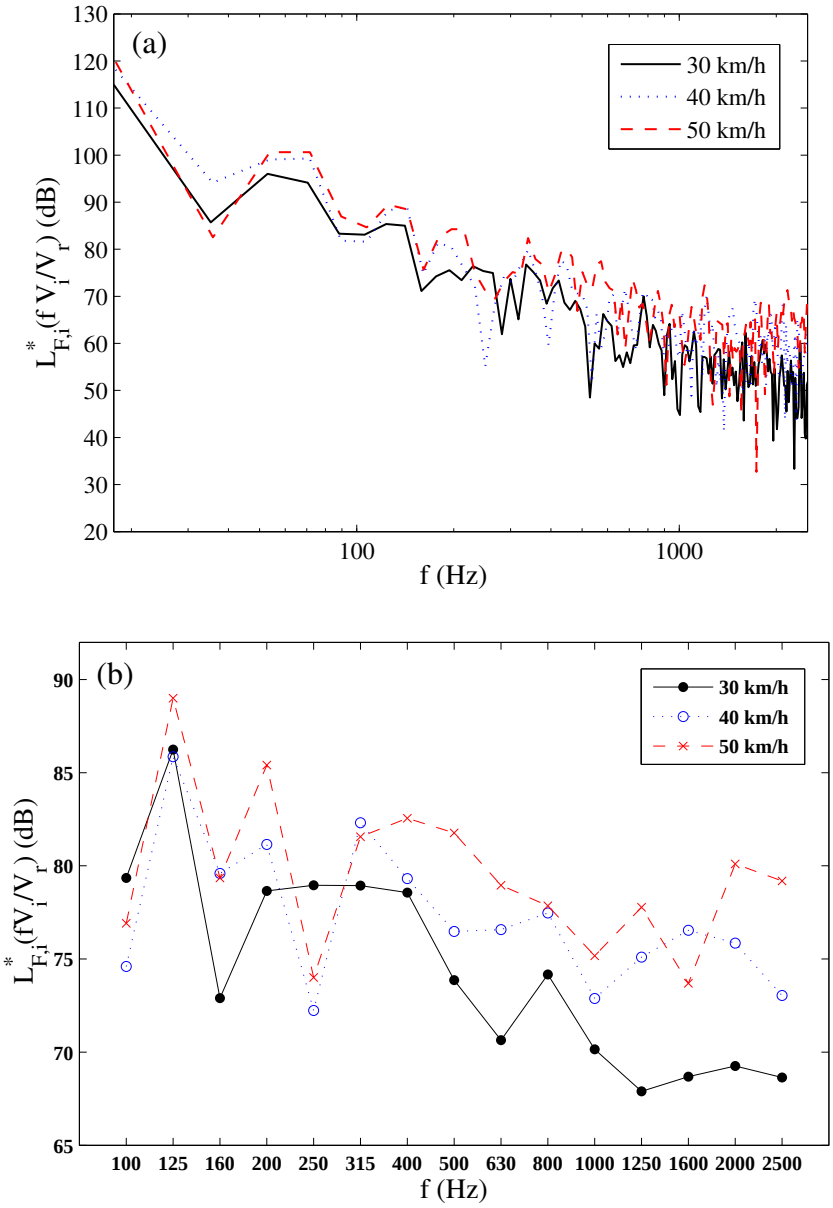

Fig. 12. Modified spectra $L^*_{F,i}$ of the resultant force at 30, 40 and 50 km/h for the DAC 0/10 (old) road surface with the reference speed V_r = 30 km/h. (a) Narrow bands levels. (b) Third octave bands levels.

42

Fig. 13. Close proximity noise measurement system (only the two side microphones have been used for the experiments).

43

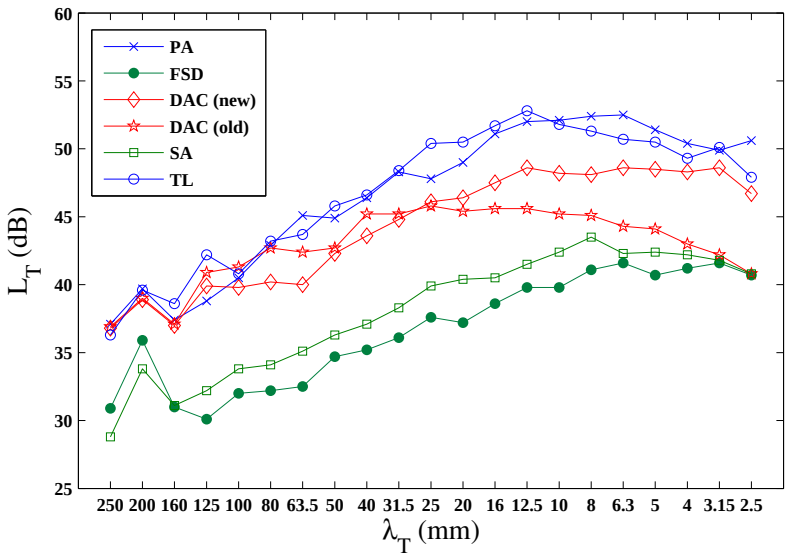

Fig. 14. Third octave bands texture levels for the six tested road surfaces.

44

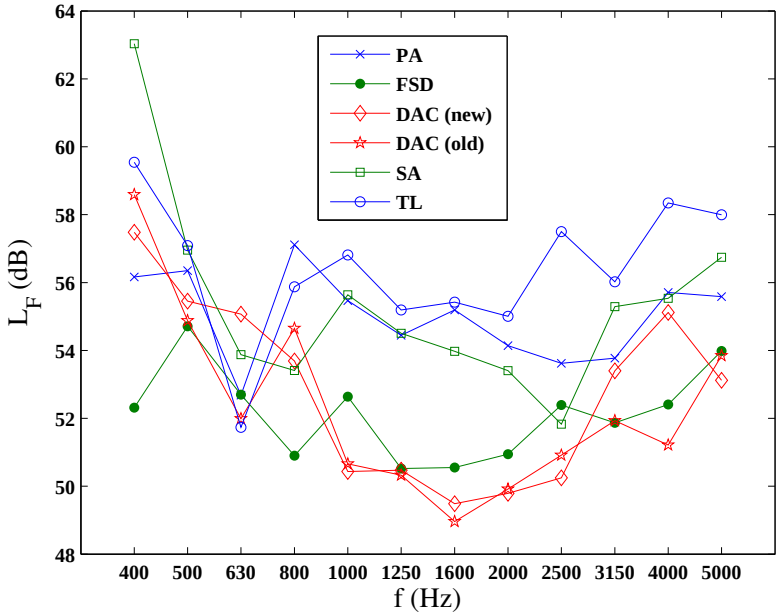

Fig. 15. Third octave bands force levels for the six tested road surfaces.

45

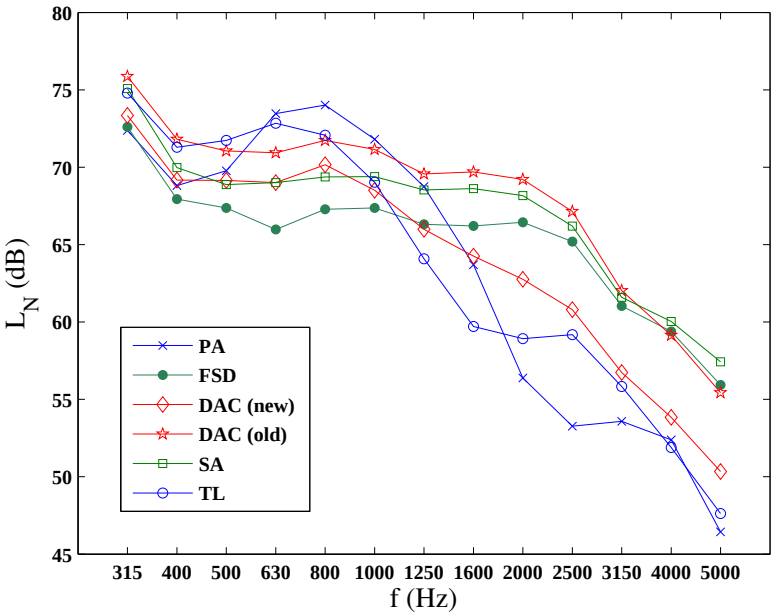

Fig. 16. Third octave bands noise levels for the six tested road surfaces.

46

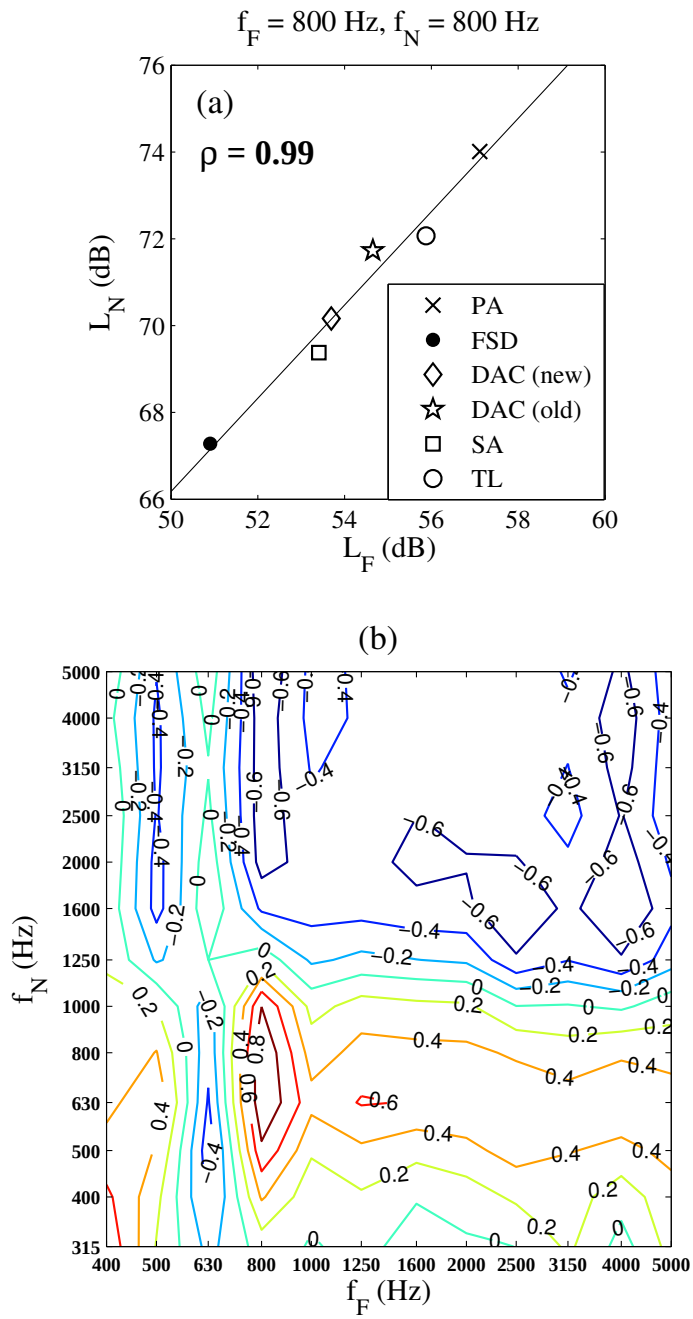

Fig. 17. (a) Correlation coefficient ρ for $f_F = 800$ Hz and $f_N = 800$ Hz, (b) Iso-correlation curves between contact forces and noise in the (f_F, f_N) plane.

47

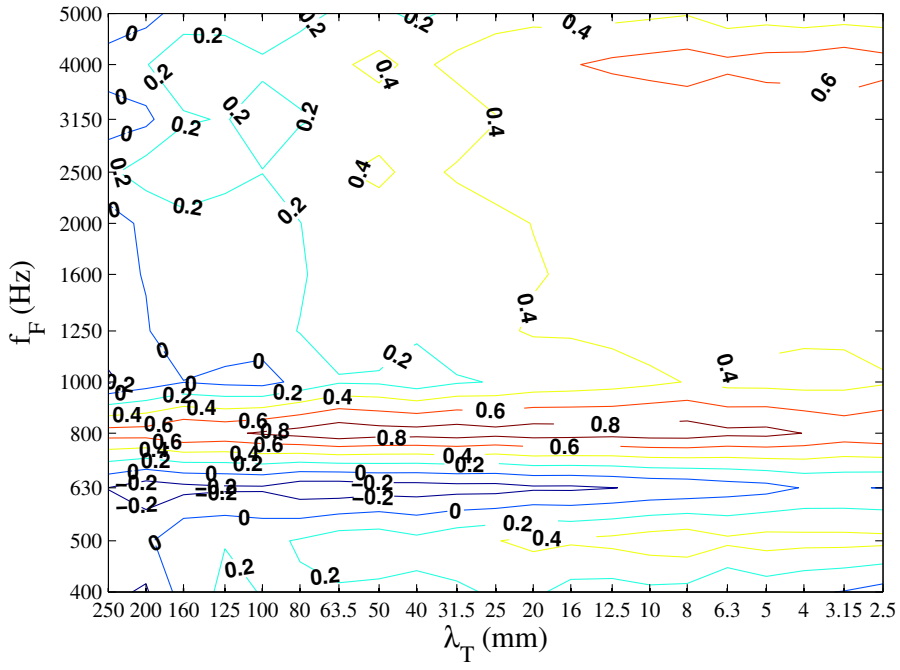

Fig. 18. Iso-correlation curves between surface texture and contact forces in the (λ_T, f_F) plane.

48

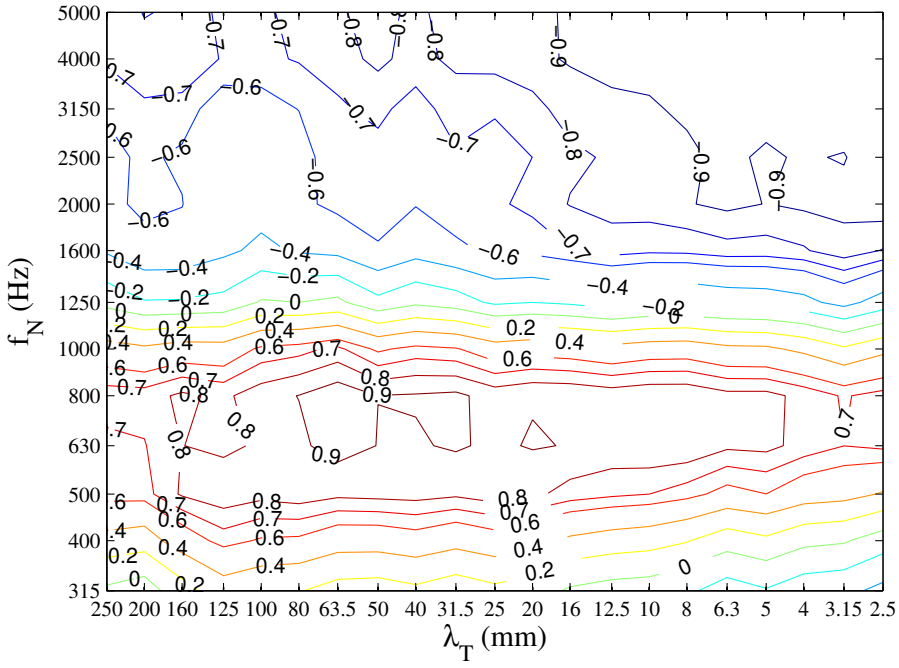

Fig. 19. Iso-correlation curves between surface texture and noise in the (λ_T, f_N) plane.

49

Road surface	Statics	30 km/h	40 km/h	50 km/h
PA 0/6	156	123	123	122
FSD 0.8/1.5	155	130	129	123
DAC 0/10 (new)	164	128	124	125
DAC 0/10 (old)	164	133	137	131
SA 0/4	160	122	127	121
TL 0/6	151	134	131	136

Table 1

Evolution of the contact area A (in cm^2) with rolling speed.

50